AN ASSESSMENT OF FORCITE APPROACHES IN PREDICTIING YOUNG'S MODULUS FROM CRYSTAL STRUCTURE

A DISSERTATION
SUBMITTED TO THE FACULTY OF THE
UNIVERSITY OF MINNESOTA
BY

Ling Zhu

IN PARTIAL FULFILLMENT OF THE REQUIREMENTS
FOR THE DEGREE OF
MASTER OF SCIENCE

Changquan Calvin Sun

July 2019

Acknowledgements

Throughout the writing of this dissertation, I have received great deal of support and assistance from people surrounding me in the past three years. Without the guidance and help from them, my investigation in pharmaceutics could be tougher and even impossible.

I would like to acknowledge my advisor Dr. Changquan Calvin Sun for his kind instruction on my project. Your expertise and working attitude really inspired me. I want to thank you for the opportunity I was given to conduct research in the Department of Pharmaceutics at University of Minnesota and the trust to explore a new research direction.

I would like to express my gratitude to Dr. Timothy Wiedmann. Your willingness and valuable guidance supported me much in both study and life. Your precious critics and opinions are essential to successfully complete my dissertation.

I also would like to thank Dr. Chenguang Wang and Dr. Shubhajit Paul. You provided me with the tools I needed to proceed on my research. Your useful suggestion kept me making progress in the project.

I was grateful for the kind assistance from my friends. Your sharing on mathematics and knowledge from your major motivated me to identify and solve the problems.

In addition, I would thank for the support from our lab members, especially Jiangnan Dun and Shenye Hu. Your patience and endeavor in instructing me to operate on lab equipment and explaining the theory behind.

Dedication

This thesis is dedicated to my wonderful, loving and supportive parents – Xinghong Zhu and Yuhong Liu

Abstract

Improving the efficiency of tablet manufacturing in pharmaceutical industry has always attracted great concern. The mechanical properties of drugs are important for successful tablet production Thus, the knowledge of mechanical properties of pharmaceutical compound in pre-formulation stage facilitates tablet formulation development. A fast and accurate computational method for predicting crystal mechanical properties from crystal structure is extremely valuable since the availability of pharmaceutical active ingredients (APIs) is usually very limited. Methods based on the potential surface energy simulation are fast but their accuracy has not been systematically evaluated using a large set of crystals. The goal of the current study was to evaluate accuracy of predicted Young's modulus (*E*) using the Forcite module in commercial software, Material Studio. The predicted *E* values of 50 organic crystals were compared to experimental values obtained by nanoindentation to assess their accuracy. A method to predict the *E* values on specific crystal faces was established to improve correlation by accounting for anisotropy of crystal mechanical properties. The correlation with experimental values remained poor. Detailed analyses of calculated *E* map of three crystals still failed to produce accurate *E*. Thus, the current Forcite module in Materials Studio for routine crystal form screening should be used with caution.

Table of Contents

List of Tables

List of Figures

1. Introduction

The tablet is the most common dosage form in the market, representing over 70% portion of all the prescribed drugs [1]. The advantages in accurate dosing, great stability, convenient manufacture procedure, low manufacture cost, patient-friendly usage and high patient compliance make it favorable to both manufacturers and patients[2]. The quality of tablet during manufacture process affects the efficacy and safety of drug products [2-6]. To improve tablet manufacturability, it is essential to understand and overcome the common problems of insufficient mechanical strength [7], punch sticking[8], and capping and lamination[9], which are discussed in more detail below.

1.1 Common problems in manufacturing process

1.1.1 Insufficient mechanical strength

Sufficient mechanical strength is the essential determinant for the successful production of a tablet[10]. It is usually measured by tensile strength, [11]which describes the maximum ability of a material to withstand the separation under a tensile stress[11].

Without enough mechanical strength, potential defect problems such as poor friability and insufficient pressure resistance[12]could take place. The friability measures the probability of a tablet to drop compound particles in the stage of abrasion and friction[13, 14]. The insufficient pressure resistance indicates the tablet is fragile and easily break up into several parts, failing for application. Both will definitely lead to unacceptable problems in downstream process such as handling, processing and packaging[15].

Factors influencing the contact areas and attraction force between particles, usually regarded as bonding area and bonding strength, will affect tablet mechanical strength[16]. As shown in the Figure 1[17], following the particle fracture, rearrangement and deformation, the bonding area reached its largest. Osei-Yeboah et al. showed that the interplay between bonding area and bonding strength affects quality of tablet during compaction. [18]. Moreover, hydrogen bonding, the weak polar interactions, the surface structure[10, 19], could also affect bonding strength. Therefore, the insufficient mechanical strength could be improved via crystal engineering[20].

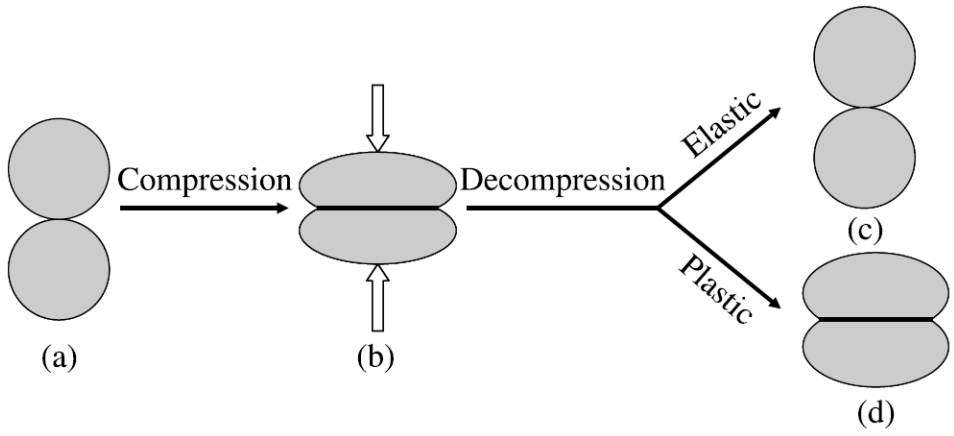

Figure 1. Deformation of particles during powder compaction.[20]

1.1.2 Punch sticking

Punch sticking is a problem occurs when powder adhere onto tooling after the compaction completed[21] (Figure 2). It is troublesome because the appearance of the tablets could be damaged and the consistency of tablet weight would not sustain[8]. Moreover, it could impede the movement of lower punches and cause damage on the press punch[22]. If a proper

solution could not be provided, both patient compliance and manufacture quality would be imparted.

One qualitative model [9]elucidated the possible mechanism of punch sticking (Figure 3). The sticking results were determined by the relative magnitude of interaction force among punch, API and excipients. It concluded that the increase of the interaction between API and excipients would effectively reduce the severity of punch sticking. One important part noticed in the model was the adhesion force. It measured the magnitude of the interaction of the contacting part among punch, API and excipients. Analyzed in the molecular level, it caused by the weak intermolecular interactions, such as van der Waal's forces, electrostatic forces and hydrogen bond[22]. The adhesion force determines the propensity where the powder particles will stay in a compaction cycle. The small adhesion between punch and API with excipient particles is desirable to reduce the remnant on the surface, but the deterioration is limited since there is a threshold of the cohesive amount as illustrated in Type I (Figure 2). The relative strong attraction within particles could be the main reason causing the overwhelming adhesion problems. This, from a view of particles, suggests that the selection of excipients could effectively improve the problems by providing appropriate mechanical strength. Similar to the case of insufficient mechanical strength problems, the modification of the morphology, surface structure and bonding strength on the compound particles could be a potential promising solution to reduce the severity of the punch sticking, making the investigation on crystal structure properties imperative.

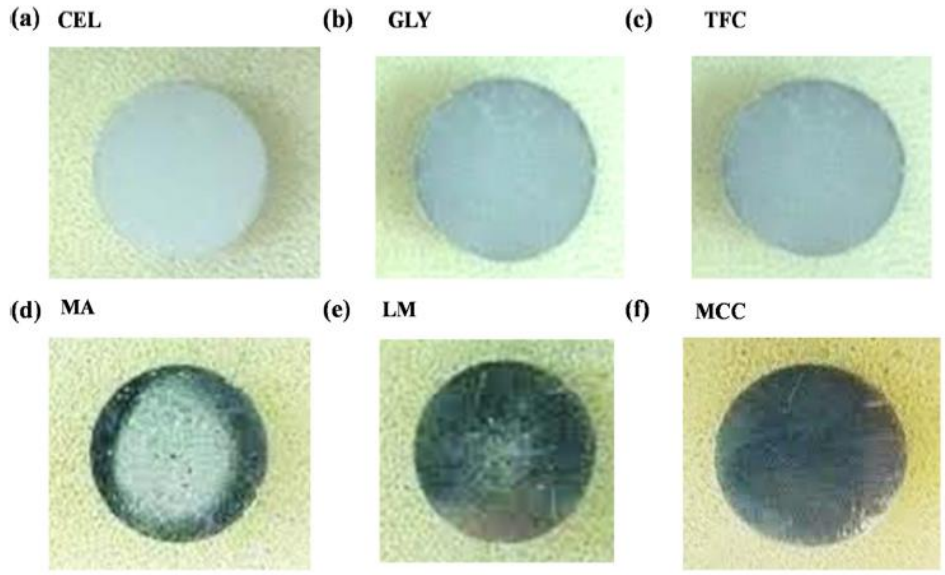

Figure 2. Image of powder adhesion on punch surface for six different compounds.[21]

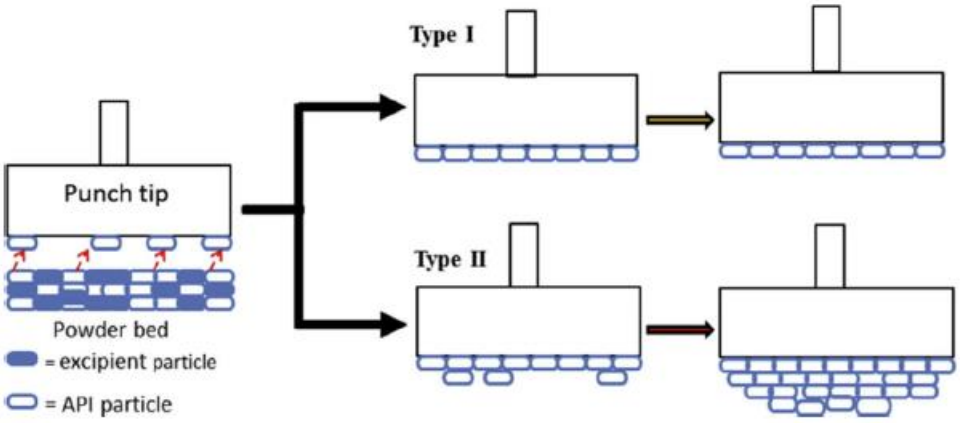

Figure 3. Schematic representation of the punch sticking kinetics based on interactive forces.[8]

1.1.3 Capping and lamination

Capping and lamination are two classical problems occurring in the stage of tablet compaction. These two problems could directly cause the tablets to the failure, leading to a great loss to the manufacturing.

While they are fracture of tablets in the compaction process, capping and lamination are two different kinds. Capping is defined as the removal of the top of bottom cups of the tablet (Figure 4a)[23]. Not just in the compaction process, but the subsequent activity such as the friability test and handling could capping be observed[21]. For the lamination, instead of splitting at the cup part, it occurs in one or multiple layers in the band parallel to the punch surface (Figure 4b)[24].

Apart from the obvious process conditions such as compression pressure[24] or speed[25], the mechanical properties of the particles also affect the quality of tablets. It is found that the capping or lamination could be induced by either external cracks or hidden cracks, [25] when exposed to an external stress. The insufficient bonding strength among particles is responsible for the capping problems. Without sufficient plasticity, the compounds would be susceptible to the lamination or capping under external stress[26]. Therefore, the modification of the mechanical strength could be a potential method to solve such problems.

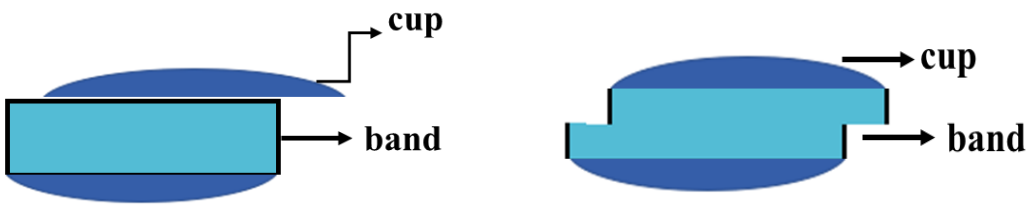

(a) (b)

Figure 4. schematic representation of (a) capping; (b) lamination

Clearly, the mechanical properties of the materials play a defining role in powder compaction[20]. Knowledge in mechanical properties of a drug in early development helps design tablet formulations free from these compaction problems. This can be achieved by computational approaches based on crystal structure.

1.2 Mechanical properties and crystal structure characteristics in tablet formulation design

In the pharmaceutical context, the behavior of drug substance in tablet manufacture process such as tableting, milling and compaction[27-30] strongly depends on the understanding of the mechanical properties, dictating the successful design of tablet formulation. As mentioned, in the process of compression, flaws such as capping and lamination could be effectively avoided if active pharmaceutical ingredient (API) could be formulated with balanced material properties excipients in the selection of excipients[31, 32]. With respect to the understanding of mechanical properties, compared to the empirical operation, the structure-properties relationship[20] has been attached importance to, a faster and more economic approach. The correlations between molecular structures and mechanical properties have been illustrated in many investigations[33-35]. The distinctive tableting performance of organic compounds in manufacture process could be elucidated by their unique crystal structures[32, 35-40]. In pharmaceutical tablet production process, a pressing requirement is the existence of satisfactory of crystal plasticity for sustaining adequate mechanical strength of tablets under compression, attracting attention on relationship between crystal structures and mechanical properties such as Young's modulus (E) and Hardness(H).

1.2.1 Tablet behaviors and mechanical properties

Modifying compaction process is a common way to improve tablet quality [25, 41]. However, like symptomatic treatment, the modification in the process can't avoid the frequent occurring problems and this process-performance leading relationship alone contribute little to understand and resolve the problems thoroughly. The mechanical properties, thus, as an "etiological treatment", has been focused on to investigate the problems in the process in a view of particles.

Several key indices used to qualify the mechanical properties of compounds are elasticity, plasticity, viscoelasticity and brittleness. They are of great importance as they determine what kind of deformation would be observed during compaction process. They intrinsically dominate the behavior of particles in the compression. For most pharmaceutical powders, they are uniformly viscoelastic and that they are viscous and susceptible to the strain rate[27]. They are prone to recover a little to the original shape after compaction, causing a partial loss of bonding area. This manifests the inherent reason impairing the tablet performance. Combined with the viscoelasticity, powders also exhibit an elastic or plastic behavior[25]. The relative preponderance between elasticity and plasticity determine the mechanical response of tablets[28]. Elasticity measures the ability to sustain the reversible deformation when applied external stress; after the stress is removed, it could completely recover to the origin without any deformation. For this reason, with small bonding area under low compress stress, the particles could hardly be compressed into a tablet and materials with high elasticity could be difficult to possess acceptable tablet performance[29]. Plasticity, the permanent deformation of the materials, is favorable for the tablet compaction. It could create a large bonding area and improve the tablet behavior, making it a critical property for tablet production[30].

From the molecular level, the mechanical properties originate from the intermolecular interaction. It includes van der Waals force, hydrogen bonding, electrostatics interaction and ionic interactions. These weak non-bond interactions play an important role in crystal packing, the arrangement of crystal unit cells. The summation of them could show attraction or repulsion tendency during deformation, affecting the mechanical response under stress. This indicates that the structure properties of the materials could cause effect on the tablet behaviors.

1.2.2 Introduction of Material Science Tetrahedron

The compaction performance is inherently associated with the mechanical properties and mechanical properties are dominated by the structure characteristics. It implies that the each of the variables could have a potential interrelationship. The concept - materials science tetrahedron (MST) [20] depicts a closely interconnection among structure, properties, processing and performance (Figure 5)[20]. The desired performance is what concerns. From the explanation of this relationship, it is dominated by the material properties, tightly linked with the structure[25]. The structure-property relationship is the focus of this work since our aim is to connect the crystal structures with mechanical properties.

The structure-property correlation allow the investigation from molecular structures to crystal packing and extend to large powder behaviors. It links the bonding strengths, bonding patterns, bonding types to the elasticity, plasticity and fragmentation, further powder flowability and tabletability.

The work that correlates the structure characteristics with the mechanical properties, such as the crystal packing and crystal brittleness[33], the interaction between crystal layers and

crystal plasticity[34], halogen bond and crystal elasticity[35]demonstrates a possibility of deducing the properties from structure-based parameters. Moreover, the probe on the relationship such as crystal brittleness[36], surface roughness[37] and moisture content[38] with powder compaction behaviors manifest the possible application of property in compaction behavior direction. Therefore, it is promising to assess the properties from the input of specific structure parameters while the concluded properties in turn direct the modification of structures and the compaction process, facilitating the final performance.

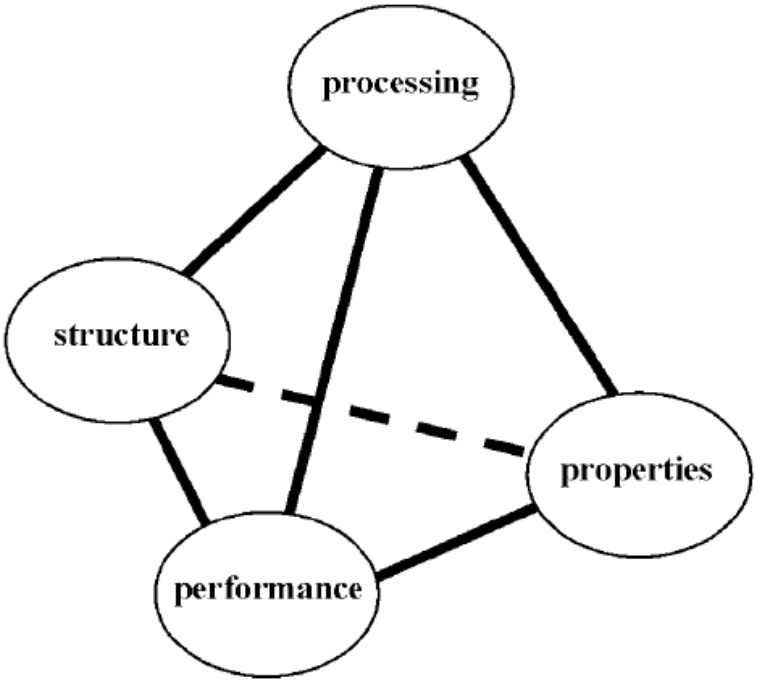

Figure 5. The materials science tetrahedron.[20]

1.2.3 Structure-property relationship studies

Most pharmaceutical compound structures are organic crystal structures that sustain the

arrangement with weak non-bond intermolecular interaction. The total intermolecular interaction in macro aspect, results in the elastic or plastic behavior of the crystals under stress, during which the molecules dislocate and the interaction change or even broke. The different arrangement of the same molecule could lead to great disparity on property like the well-known example graphite and diamond[39]. Similar to this,the different properties from polymorphs of the same organic crystal make it imperative to investigate the influence of the interaction.

Several cases demonstrate the tight linkage between structure and property. One example is sulfamerazine[40]. The interesting part of this compound is the obvious difference on plasticity of different crystal forms. In the Form I (Figure 6a)[40], the molecules associated with hydrogen bonding made into sperate layers and each layer as a unit constituted the whole structure in a two-dimensional view. Each layer shaped as a flat plane and loose space could be observed between each layer. Based on the slip mechanism, like the structure of graphite, these flat planes with weak inter-plane interactions were expected to slide easily and indeed had superior plasticity[40]. While for Form II (Figure 6b)[40], the crystal stacks were closer and interlock with each other in a zigzag shape. Thus, this tight interaction between layers prevented the separation and presented a smaller plasticity than Form I.

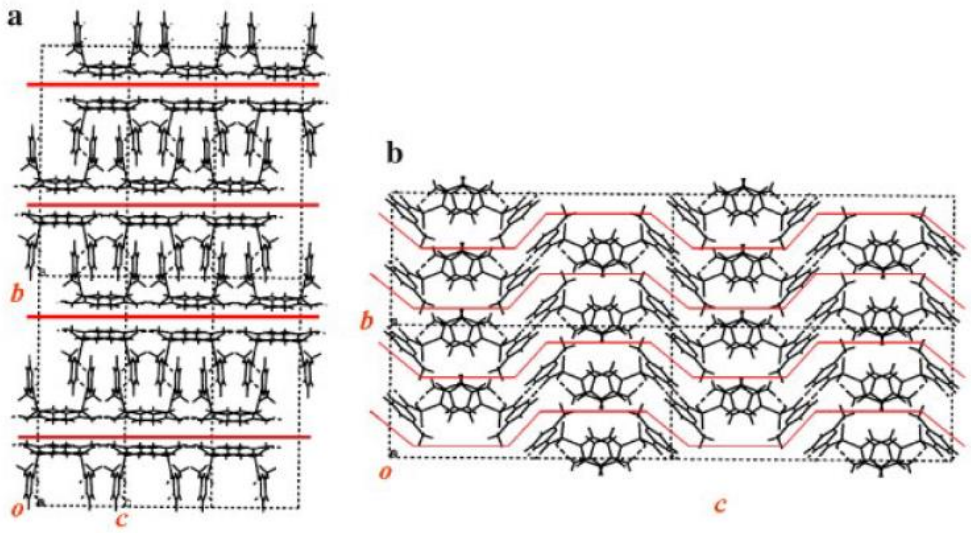

Figure 6. Crystal structures of sulfamerazine polymorphs (a) form I; (b) form II.[39]

Similar to the sulfamerazine case, the study on anhydrate *p*-hydroxybenzoic acid form and monohydrate form showed comparable discrepancy in plasticity[41]. The anhydrate form was composed of several comb-like layers (Figure 7a)[41] and made it difficult to slip, leading to a small plasticity. With the addition of water molecules between the adjacent layers, the plasticity and tabletability were improved [41].

These studies strongly suggest the intimate relationship between crystal structure and mechanical property, which suggests the possibility of improving mechanical properties of drugs through crystal engineering.

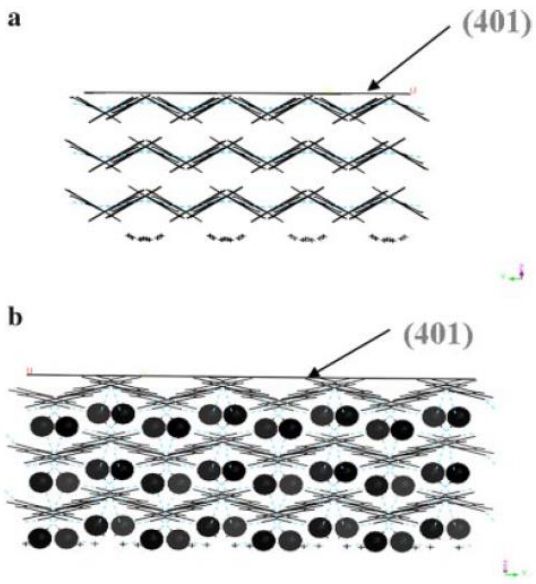

Figure 7. Crystal structures of *p*-hydroxybenzoic acid (a) anhydrate form; (b) monohydrate form.[40]

Apart from the influence on the plasticity from layers interaction, the work on 4-Chlorophenyl 4-bromobenzoate illustrates the influence on elasticity and plasticity within layers (Figure 8)[42]. The fascinating part is the hand-twisted helical property of the structure. The possible mechanism was the existence of the halogen bond and π-π interaction within the structure. The π-π interaction functioned as a spring to store the deformation force and the limitation was determined by the bond angle and distance of the halogen bond[42]. The tolerance of the halogen bond on the change of angel and distance decided the magnitude of the elastic response and occurring of plasticity[42].

This study indicates that if the parameters of the structure could be fully utilized, the prediction on the mechanical behaviors is anticipated.

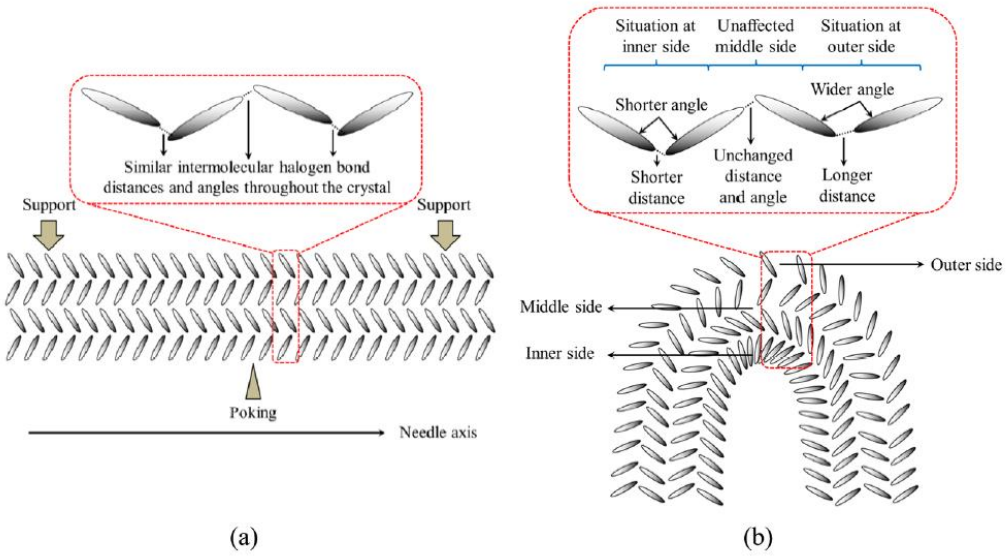

Figure 8. schematic representation of the bending mechanism (a) before bending; (b) after bending.[42]

1.2.4 Relationship between Young's modulus (*E*), Hardness (*H*) and crystal structures

For pharmaceuticals, the investigation of mechanical performance is of practical importance because of the involvement of mechanical operation in industry process[10]. Plastic deformation is the fundamental measurement of the tableting property[17], and Hardness (*H*) defines the resistance to plastic deformation of materials. . In view of molecular crystal structure, Hardness is strongly related to the existence of the slip planes, whose ease of sliding dominated by the intermolecular energy between layers and to the defects motion within crystal lattices[34].However, little reliable hardness (*H*) data for pharmaceutical compounds are available and the assessment of each pharmaceutical compound on hardness (*H*) is distinctive and complex. Thus, Young's modulus(*E*), which measures the resistance of material against elastic deformation, is introduced as a mean to evaluate *H*, since it is also a material-based quality and relevant to the crystal structure It

is determined by the curvature of the potential energy curve at the energy minimum[43], influenced by intermolecular interaction. Several calculated methods have been used to predict reasonable values of E[44, 45]from crystal structures, indicating a possible method for easier and faster prediction of material behavior. A work [46] (Figure 9), has shown an excellent correlation between E and H, suggesting that the E could be used for the prediction of H. Based on that, a potential valuable mathematic model of H prediction could be established.

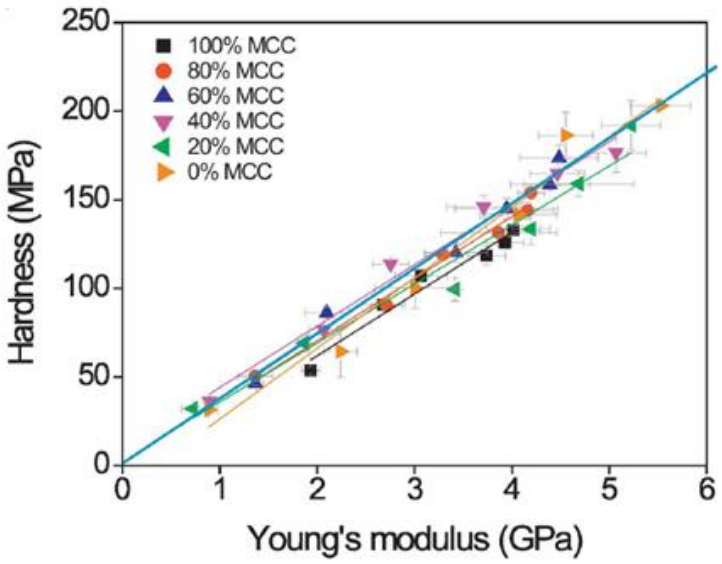

Figure 9. Relationship between hardness and Young's modulus of MCC, DCPA and their mixtures.[46]

1.3 *In silico* model for the prediction of Young's modulus

Because the sufficient drug substance is not always available in the pre-formulation phase and the cost could be even higher for novel products, a requisite for the assisting formulation design in a more beneficial approach is demanded. An attainable

computational method rather than experiment is of more interest. It requires less drug compound consumption and makes it easier to measure mechanical properties in early formulation design. For experiment, high crystal quality is needed and the test is easily influenced by the ambient conditions[48,49]. Different from that, a computational method could directly quantify the mechanical properties from crystal structures. The application of the computational method, as a substitute, could also avoid the problem from the compaction simulation data analysis[47] and provide reliable prediction of mechanical properties based on the crystal attributes.

Meanwhile, a faster formulation design would be favorable in market competition. Thus, the Forcite modulus an available *in silico* models in commercial software, Material Studio is applied to simulate the mechanical properties of crystals. It is based on the molecular mechanical calculation, considering just geometry of crystal structure and ground state energy without electrons[48]. The model could provide a quick prediction of *E* from a determined crystal structure while sacrificing some accuracy.

Since few studies have identify the effectiveness of this *in silico* model, it is imperative to validate the results of this calculation method and evaluate the possible application in facilitating formulation design.

In this work, we systematically investigated the Forcite module and operated it under various force fields and charges. While *E* is easily measured, it was used as a mainly index to estimate the accuracy of the model and assessed by comparing to experimentally

determined value. The experimental results were generally determined by nanoindentation from different reference. This is because nanoindentation is considered the one with high accuracy and precision. The relation between the calculated and experimental *E* values are used to assess the accuracy of the Forcite module. If there is a strong correlation between them, the method is validated.

1.4 Determination of Young's modulus from nanoindentation

In this study, the results of *E* from nanoindentation test was used to verify the accuracy of the computational model. This technique was considered to be capable to provide precise and quantitative results on small-volume materials mechanical response[49] and recently applied to mechanical properties characterization of organic pharmaceutical crystals[38, 50-52].

The loading-displacement curve (Figure 10)[53] typically from the experiment is used for obtaining the mechanical properties and in our work mainly the Young's modulus. The first important parameter from the curve is the contact stiffness (S) defined as the slope of unloading curve in the upper part. It could be deduced from the derivative of load (P) and displacement (h) as shown in Eq.1.

$$S = \left(\frac{dP}{dh}\right) \qquad \text{Eq.1}$$

The mechanical properties such as *H* and *E* then would be computed by following the standard method settled by Oliver-Pharr[54]. For the calculation of *E*, several parameters are required, including, the depth of contact (h_c), the contact area (A_p,), and the reduced Young's modulus (E_r).

The parameter h_c is determined by the indenter displacement at loading peak and contact stiffness according to Eq.2.

$$h_c = h_{max} - \varepsilon\left(\frac{P_{max}}{S}\right) \quad \text{Eq.2}$$

The ε is a constant determined by the indenter shape and for Berkovich indenter.

For Berkovich indenter, the A_p is a function of contact depth h_c illustrated in Eq.3

$$A_p = 24.56{h_c}^2 \quad \text{Eq.3}$$

Then the E_r could be calculated from all the above parameters by Eq.4

$$E_r = \frac{\sqrt{\pi}}{2\beta}\frac{S}{\sqrt{A_p(h_c)}} \quad \text{Eq.4}$$

The β is an indenter-shape-based factor and take elastic deformation of both sample and indenter into consideration. The value of β for Berkovich indenter is 1.034.

By Eq.5, *E* could be deduced

$$\frac{1}{E_r} = \frac{1-{v_s}^2}{E} + \frac{1+{v_i}^2}{E_i} \quad \text{Eq. 5}$$

v_i and E_i represents the Young's modulus and Poisson's ratio of indenter separately; the v_s is defined as the Poisson's ratio of tested samples.

From the above equations combined with experiments, the *E* could be acquired precisely in a nanoscale, leading to an investigation of relative strength of intermolecular interaction[43].

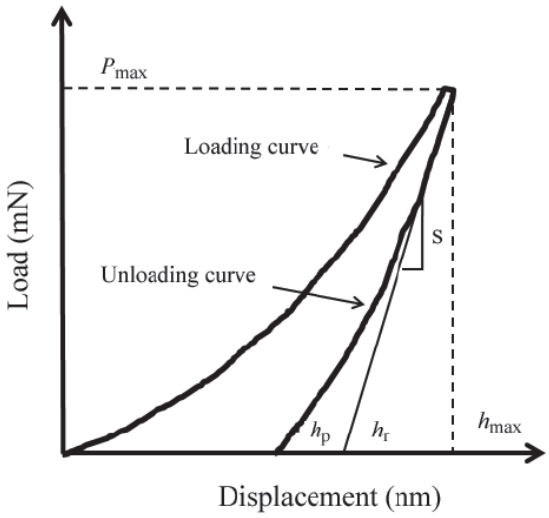

Figure 10. Load-displacement curve (h_p – permanent depth after removal of test force; h_r – intersection of the tangent to the first part of the unloading curve with the displacement axis; h_{max} – indenter displacement at peak load).[53]

2. Materials and methods

2.1 Materials

Both crystalline excipients and APIs were involved in this project, such as sucrose, aspirin and β-piroxicam. Their crystal structures were downloaded from the Cambridge Crystallographic Data Centre (CCDC). experimental *E* were obtained from the literature.

2.2 *In silico* model for Young's modulus prediction

The elastic tensors of a given crystal were calculated using the Forcite module in Materials Studio 2016 (BIOVIA Inc., San Diego, CA). Different force fields including Compass II, Drieiding, pcff and Universal and various charges, such as Force field assigned, Qeq, and Gasteiger, were used for the calculations. The simulation was operated at ultra-fine quality. In all the calculation groups, the electrostatic method summation was settled "Ewald" and the van der Waals summation was selected as "atom based". Geometry optimization of the

crystal structure was performed before calculation and the smart algorithm was chosen during all the processes. The energy was set at $2*10^{-5}$ kcal/mol with force at 0.001 kcal. mol -1. $Å^{-1}$ and displacement at 10^{-5} Å as the converge conditions of the atom-based geometry optimization, while the unit cell was set as unoptimized. The mechanical properties were acquired by applying specific simulated strains to the crystal structure, and the number of strains was selected as four to increase the accuracy of results and avoid the generation of undistorted structures. The Maximum strain was 0.003 for the maintenance of linear elasticity of structures and demonstration of the structure property.

2.3 Elastic Constants Calculation for specific crystal faces

A 6 × 6 stiffness matrix within the calculated results was used to describe the stress-strain

$$\begin{bmatrix} \sigma_1 = \sigma_{xx} \\ \sigma_2 = \sigma_{yy} \\ \sigma_3 = \sigma_{zz} \\ \sigma_4 = \sigma_{yz} \\ \sigma_5 = \sigma_{xz} \\ \sigma_6 = \sigma_{xy} \end{bmatrix} = \begin{bmatrix} C_{11} & C_{12} & C_{13} & C_{14} & C_{15} & C_{16} \\ C_{21} & C_{22} & C_{23} & C_{24} & C_{25} & C_{26} \\ C_{31} & C_{32} & C_{33} & C_{34} & C_{35} & C_{36} \\ C_{41} & C_{42} & C_{43} & C_{44} & C_{45} & C_{46} \\ C_{51} & C_{52} & C_{53} & C_{54} & C_{55} & C_{56} \\ C_{61} & C_{62} & C_{63} & C_{64} & C_{65} & C_{66} \end{bmatrix} \begin{bmatrix} \varepsilon_1 = \varepsilon_{xx} \\ \varepsilon_2 = \varepsilon_{yy} \\ \varepsilon_3 = \varepsilon_{zz} \\ \varepsilon_4 = \varepsilon_{yz} \\ \varepsilon_5 = \varepsilon_{xz} \\ \varepsilon_6 = \varepsilon_{xy} \end{bmatrix}$$

behavior of the various crystal structures. Due to the matrix symmetry, the maximum of 21 coefficients are needed for the description of stiffness behavior[55]. The ELATE, an open source calculation module[56] was used to analyze the second-order stiffness matrix and visualize the output of the elastic properties. One translational model was used to convert the fractional coordinates of each crystal to Cartesian coordinates where the stiffness matrix and ELATE demonstrated the results. The crystal face of a crystal, denoted with the Miller indices (h k l), could be expressed as h$\boldsymbol{a}$ + k$\boldsymbol{b}$ + l$\boldsymbol{c}$ in specific fractional coordinates, where *a*, *b*, and *c* are crystal unit cell dimensions. In the Cartesian coordinates, three

mutually perpendicular vectors, h'$\boldsymbol{e_1}$ + k'$\boldsymbol{e_2}$ + l'$\boldsymbol{e_3}$, represented the same crystal face, where h', k', l' are components and $\boldsymbol{e_1}$, $\boldsymbol{e_2}$, $\boldsymbol{e_3}$ are bases[57]. Thus, equation 6 may be written:

$$(h \quad k \quad l) * \begin{bmatrix} \vec{a} \\ \vec{b} \\ \vec{c} \end{bmatrix} = (h' \quad k' \quad l') * \begin{bmatrix} \overrightarrow{e_1} \\ \overrightarrow{e_2} \\ \overrightarrow{e_3} \end{bmatrix} \qquad \text{Eq. 6}$$

the $\vec{a}$, $\vec{b}$, $\vec{c}$ represents the basis vectors which are unit lattice translation vectors, defining the coordinate axis of distinct crystal structures and the h k l denoted the Miller indices of the planes in the crystal coordinates.
$\overrightarrow{e_1}$, $\overrightarrow{e_2}$, $\overrightarrow{e_3}$ represented the basis vectors in the cartesian coordinates and h' k' l' denoted the Miller indices in the Cartesian coordinates after translation.

To solve the value of (h' k' l') applied in ELATE, both sides of Eq. 6 multiply by $[\overrightarrow{e_1} \quad \overrightarrow{e_2} \quad \overrightarrow{e_3}]$ to obtain Eq. 7:

$$(h \quad k \quad l) * \begin{bmatrix} \vec{a} \\ \vec{b} \\ \vec{c} \end{bmatrix} * [\overrightarrow{e_1} \quad \overrightarrow{e_2} \quad \overrightarrow{e_3}] = (h' \quad k' \quad l') * I3 = (h' \quad k' \quad l') \qquad \text{Eq. 7}$$

Therefore, Equation 8 can be obtained:

$$(h' \quad k' \quad l') = (h \quad k \quad l) * \begin{bmatrix} \vec{a} \cdot \overrightarrow{e_1} & \vec{a} \cdot \overrightarrow{e_2} & \vec{a} \cdot \overrightarrow{e_3} \\ \vec{b} \cdot \overrightarrow{e_1} & \vec{b} \cdot \overrightarrow{e_2} & \vec{b} \cdot \overrightarrow{e_3} \\ \vec{c} \cdot \overrightarrow{e_1} & \vec{c} \cdot \overrightarrow{e_2} & \vec{c} \cdot \overrightarrow{e_3} \end{bmatrix} \qquad \text{Eq. 8}$$

The triclinic crystal system is of the lowest symmetry among all crystal systems. Thus, a solution for the triclinic crystal system can be applied to all other crystal systems. For a triclinic crystal system, 21 coefficients are needed to fully describe the stiffness matrix. In Materials Studio, the axis ***c*** aligns with the z axis and ***a*** lies in the xz plane[48], as shown in Figure 11.

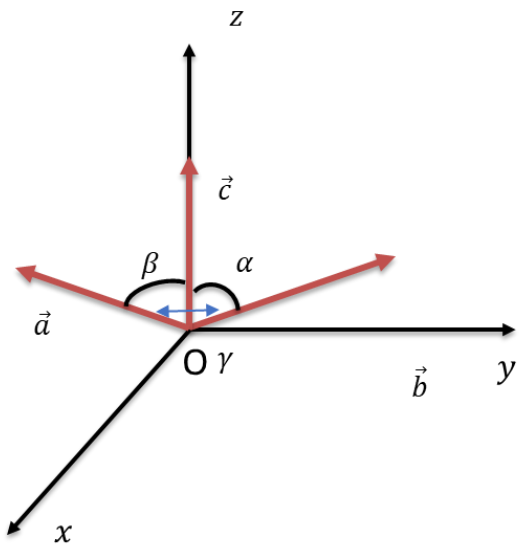

Figure 11. Schematic representation of transformation of fractional coordinates to Cartesian coordinates

Thus, the vectors ***a*** and ***b*** in the crystal can be translated into the Cartesian system using equation 9.

$$(h' \quad k' \quad l') = (h \quad k \quad l) * \begin{bmatrix} |a|\sin(\beta) & 0 & |a|\cos(\beta) \\ |b|\sin(\alpha)\cos(\delta) & |b|\sin(\alpha)\sin(\delta) & |b|\cos(\alpha) \\ 0 & 0 & |c| \end{bmatrix} \quad \text{Eq. 9}$$

Where $\cos(\delta) = \frac{\cos(\gamma)-\cos(\alpha)\cos(\beta)}{\sin(\alpha)\sin(\beta)}$; β denotes the angle between ***a*** **and** ***c***; α denotes the angle between ***b*** **and** ***c***; γ denotes the angle between ***a*** **and** ***b***. For the most common monoclinic crystal system, both α and γ are equal to 90 degree, indicating the *b* axis is aligned with the y axis. Therefore, equation 9 is simplified into equation 10.

$$(h' \quad k' \quad l') = (h \quad k \quad l) * \begin{bmatrix} |a|\sin(\beta) & 0 & |a|\cos(\beta) \\ 0 & |b| & 0 \\ 0 & 0 & |c| \end{bmatrix} \quad \text{Eq. 10}$$

The results of *E* solved by the ELATE from stiffness matrix is shown as a distribution of *E*-map in three-dimensional view in the Cartesian coordinates. To obtain *E* for a crystal face with the Miller indices of (h k l), the direction perpendicular to that crystal face can be identified by two angles, θ and φ. The two angles define a line that crosses the *E* surface map at the value corresponding to the *E* of that specific (h k l) crystal face. One example is shown in Figure 12, where θ denotes the angle between the specific crystal direction and z axis and φ denotes the angle between the x axis and orthogonal projection of crystal direction on xy plane (Figure 13).

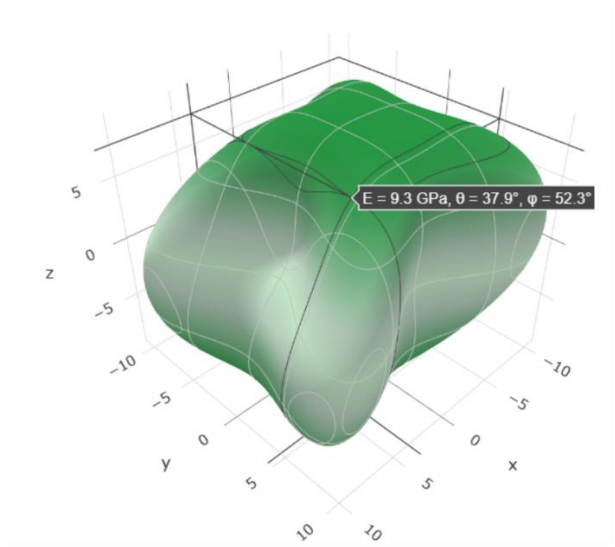

Figure 12. One example of *E* distribution by ELATE.

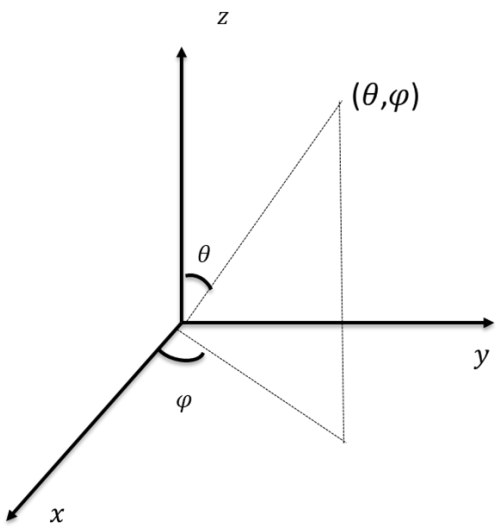

Figure 13. Schematic representation of transformation of Cartesian coordinates to Spherical coordinates.

.

Based on the Cartesian coordinates translated from the coordinates of a specific crystal face, the value of θ and φ are obtained from $(h' \quad k' \quad l')$ using equations 11 and 12.

$$\theta = cos^{-1} \frac{1}{\sqrt{(h'^2+k'^2+l'^2)}} \qquad \text{Eq. 11}$$

$$\varphi = cos^{-1} \frac{1}{\sqrt{(h'^2+k'^2)}} \qquad \text{Eq. 12}$$

With the specific values of θ and φ, the value of *E* could be easily found on the *E* distribution map generated by ELATE.

3. Results

3.1 Selection of optimum modeling for calculated Young's modulus

In the view of mechanical mechanics, Young's modulus is defined by the second-derivative of the force-distance curve at the lowest energy point[43]. This is represented by the approximation of the potential surface energy in the Forcite module, relative to the movement of atomic nuclei[48]. Considering that the force field and charge played a vital role in describing the potential surface energy of molecular crystal structures, it is imperative to determine a suitable group for the force field and charge for optimization in the simulation of mechanical properties.

In order to evaluate the accuracy of each group method, 20 compounds including both excipients and APIs were selected for the test of methods, among which, 11 were neutral compounds, 4 were salts, 3 were cocrystals and 2 were hydrates. Each compound was optimized by 10 different combinations of force fields and charge to simulate the potential surface energy and calculated to acquire the Young's modulus. The combination was considered improper for the crystals, if the generated *E* was negative or the simulation failed in the process, which indicates that structures were unstable. The initial selection of the method was then based on the success rate of acquiring reasonable results of *E* (Table 1). One unanticipated finding was that among the 10 groups of force fields and charge, only two combinations, COMPASS II with Qeq and PCFF with Qeq, could provide acceptable *E* values with 95% and 90% success rate separately out of 20 various pharmaceutical compounds. Consequently, it was expected that these two combinations

could potentially generate more reliable results from crystal structures for more compounds, and thus they were chosen for further selection of methods.

Table 1. Predicted Young's Modulus with 10 combination methods in Forcite Module from 20 crystal structures

force field	charge	number of unstable Young's modulus	success rate of acquiring results (%)
COMPASS II	Forcefield assigned	4	80%
	Qeq	1	95%
	Gasteiger	8	60%
PCFF	Forcefield assigned	4	80%
	Qeq	2	95%
	Gasteiger	6	70%
Universal	Qeq	10	50%
	Gasteiger	10	50%
Direiding	Qeq	5	75%
	Gasteiger	9	55%

Another 30 pharmaceutical compounds were introduced to compare the reliability of the two combinations. From the success rate of acceptable *E*, both combinations have a satisfactory simulation and no obvious discrepancy could be observed (Table 2). A further comparison was required to determine the optimum combination of force fields and charge. The experiment results of *E* from nanoindentation were considered a more accurate measure[43] and were used to evaluate the calculated results. Due to the low symmetry of the molecular crystals, the *E* from the simulation results was shown in three distinctive values with respect to the crystal directions. The algorithm average method was then operated to analyze the diverse elastic moduli[33]. The results of the comparison between the experiment

results and each model combination are displayed in Figure 14. The slope of the calculation *E* with combination of COMPASS II and Qeq versus experiment results was 0.612, and the adjusted R-squared was 0.56. For the combination of PCFF and Qeq, the slope was the same as the COMPASS II with a value of 0.612, while the adjusted R-squared was a little lower, with the value of 0.529.

Both methods showed that there is a correlation between prediction and experiments, but none of the two combination methods demonstrated a perfect prediction based on the expectation that the slope should be close to one with a high adjusted R-squared, since in the ideal situation the calculated is identical with the experiment. It was also found that most points were distributed in the lower part of the plot with a comparably small *E*, and they scattered equally along the prediction line, suggesting that the points with high *E* value primarily affected the linearity of the regression line, and the coarse estimation may decrease the linearity without the high *E* value points.

As shown in the Figure 15 for the COMPASS II group, sample 15 is an influential point with its location in the upper part of the plot with an *E* value of 35 GPa. When the point was eliminated, the slope of the prediction line decreased to 0.524, with a reduction of adjusted R square to 0.48 (Figure 16). For the PCFF combination, it was similar that the prediction line slope declined to 0.484 with the adjusted R square to 0.46 without the influential point, which also had a large *E* value. It was observed that no matter with or without the influential points, the predicted values from the regression line were around half of the experiment results, indicating a larger disparity of Young's modulus value on the molecular crystals between prediction and experiment. Moreover, for some compounds, the range of the difference between the calculated results and the experiments was more

than 10 GPa. This greatly affected the approximation of the pharmaceutical compounds, because most of them were organic compounds with a relatively small *E* value[43] and several unit variations on numerical value could lead to different qualification of the crystal mechanical property. However, even the prediction was not precise as expected, the existing correlation illustrated the promising application of the methods . More investigation is required for the selection of better combination of forcefield with charge. Yet, based on the statistical results, the superiority among the two combinations with force fields and charge was difficult to differentiate due to the small difference of adjusted R-squared and the slope without influential points. This was not unexpected, because these two force fields were developed from the CFF91 forcefield[58, 59] with extended coverage on various molecules such as organic materials. While compared to PCFF, the COMPASS II forcefield included the parameters from condensed phase properties and was applicable in a larger range of molecules, indicating that it was potentially more applicable to investigate further in the research of solid pharmaceutical compounds.

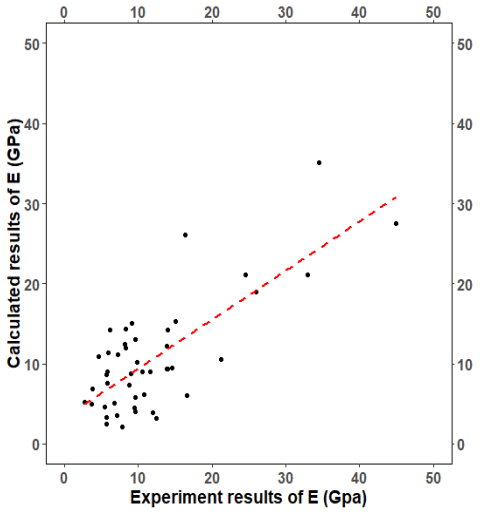

(a)

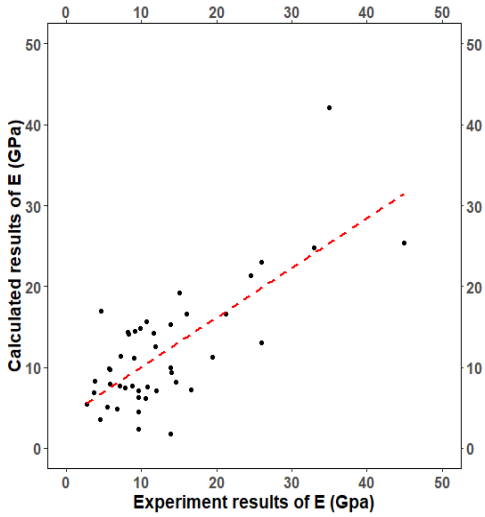

(b)

Figure 14. Young's modulus (*E*) from calculated method versus experiments: (a) COMPASS II and Qeq; (b) PCFF and Qeq

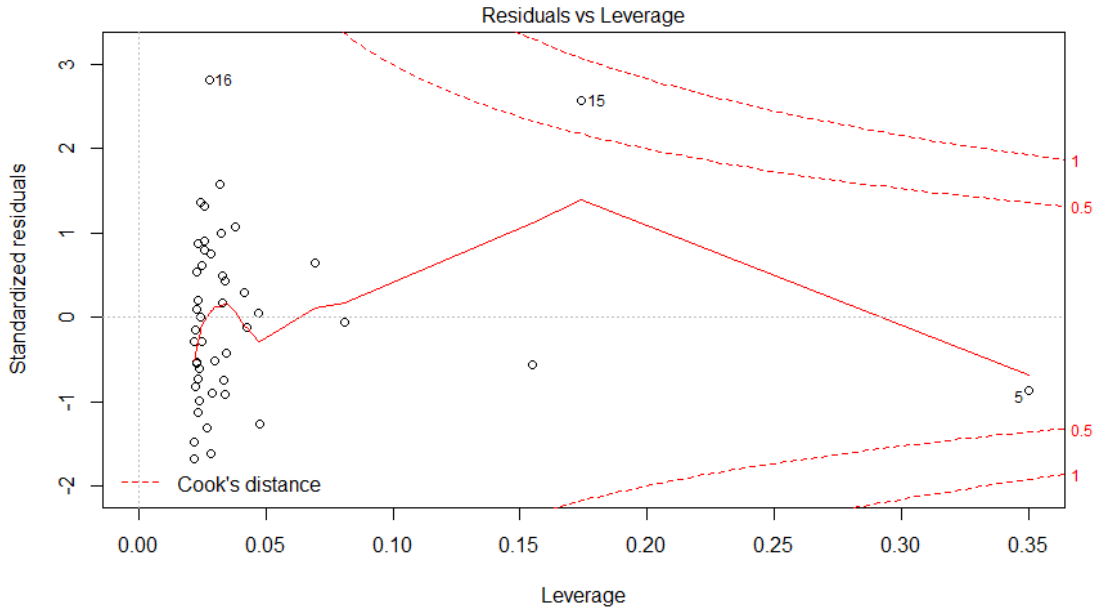

Figure 15. Residuals versus leverage from linear regression diagnostic plot based on COMPASS II with Qeq

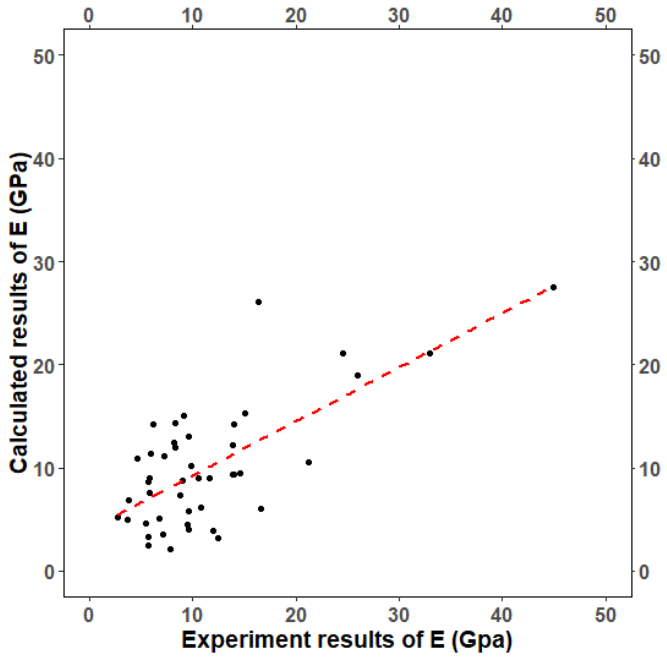

Figure 16. Young's modulus (*E*) from calculated method versus experiments without influential point based on COMPASS II and Qeq

Table 2. Predicted Young's Modulus of Crystals by COMPASS II and PCFF with Qeq in Forcite Module from 50 crystal structures

force field	charge	number of unstable Young's modulus	success rate of acquiring results (%)
COMPASS II	Qeq	4	92%
PCFF	Qeq	5	90%

In a conclusion, the combination of COMPASS II and Qeq was selected as a potential optimum condition for the optimization of the structure and further the prediction of Young's modulus from more molecular crystals. However, more operations were required to improve the accuracy of the simulation method, especially for specific crystals.

3.2 Prediction of facet specific Young's modulus from elastic matrix

In the previous part, we found that the existence of large *E* values strongly affected the slope of the regression line. In order to acquire a convincing comparison trend, more crystal structures in the upper part of the plot should be included to calibrate the regression line. However, few pharmaceutical compounds are available with relatively large *E* values. This is because organic crystals were combined with intermolecular interactions, a weak interaction force to sustain the crystal packing[60-62], and *E* was mainly determined by the nature of chemical bonds. As such, it would be difficult to involve more organic compounds with large *E* value into the data group.

Instead of adding more compounds with large *E* values, optimizing the analyzing process was considered a potential solution for acquiring more accurate results. Based on the crystal anisotropy, various statistical methods were applied to deal with the values from three distinctive directions and balance the influence from the lack of symmetry. As the *E* values of the same crystal structure could largely diverge in three directions, and the face dominated the general property of *E* was unclear, both root square mean and harmonic average were chosen to estimate the general *E* of each compound and compared with the experiment results. Figure 17 displays the results of the two statistical methods, where the slope of the predicted line based on square root mean was 0.687 and the adjusted R square was 0.557 while for the harmonic mean value, the slope was 0.481 with a 0.532 adjusted R square value. Compared with the average method, the regression line from square root mean exhibited a higher slope value, closer to 1 with comparable adjusted R square value. However, the combination may still be insufficiently accurate to simulate the Young's modulus of crystals, as the prediction slope was still smaller than 1 and the points in the lower part of the plot dispersed around the line. The problems illustrated in the average method still existed in the two statistical methods, such as the coarse approximation of *E* in specific single crystal point.

The variation in the slope and adjusted R square value in different statistical methods indicated that the anisotropy of the crystal played an important role in determining the property of *E*. Within the same crystal structure, the anisotropy can affect the quantification of *E* and thereby affect estimation of the mechanical behavior. Due to the lack of the accuracy and precision in prediction of *E*, general statistical methods were unlikely to

provide satisfactory results for each crystal. Thus, instead of describing the molecular crystal properties in simple terms, the assessment of the *E* was operated independently based on specific face of each molecular crystals, which was in accordance with the test results from nanoindentation[43].

To analyze the crystal facet specific *E*, the elastic matrices from the simulation output were introduced to calculate the specific *E*. In this process, the face direction of each crystal was transformed from specific fractional coordinates into the Cartesian coordinate, and the interpretation of *E* was then performed in the same coordinate system. Since the focus on *E* was changed from the general structure to a specific face of crystal, the comparison between the experiment and prediction could be performed directly without applying different statistical methods. The evident problem for this method was that the available number of *E* on specific face in the aforementioned crystal structure database was quite limited. Only few pharmaceutical compounds were examined specific facet *E* values by experiments. Thus, a regression line was established on multiple available *E* on different faces of crystals.

As shown in the Table 3, what unexpected was that several structures that could get simulating results from direct results were unstable and could not get *E* values when simulating *E* with elastic matrices. The results suggest that even the chosen combination of forcefield COMPASS II and charge Qeq could not guarantee a successful prediction, when exploring the face-based *E* property. A regression line was used to assess whether there was any improvement in the comparison between simulation results and experiments.

It was found that the slope of the regression line was 0.577 and adjusted R square 0.354, both even lower than those from the statistical methods, indicating the limit accuracy of this simulation method (Figure 18). However, when inspecting the plot, except for several points away from the line with large prediction *E* values, the remaining points were concentrated near the regression line compared with the plots achieved in the statistical methods. It was also found that several points with high large experiment *E* values influenced the characterization of the regression line and when those points were removed, the slope of the line was 0.71 with adjusted R square value equaling to 0.5 (Figure 19). It indeed showed some improvement of the prediction in the slope of the regression line when the comparison was made based on specific face. However, due to the existence of points with high prediction *E* value, an improvement of the prediction accuracy from the increase of the slope could not be concluded; the value of adjusted R square was also small and not reflected in the concentration of the points along the line.

Therefore, the accuracy was still not satisfactory for the prediction when compared on single crystal point. From the above analysis, the combination with forcefield COMPASS II and charge Qeq could not provide a perfect prediction of *E* from crystal structures, and it was speculated that for other combinations of forcefield and charge, a satisfactory simulation of *E* was difficult to obtain. However, given the change of the figure characteristics from general analysis to specific face simulation, the application of Forcite modulus on individual crystal structures to evaluate the accuracy was explored further, and the potential drawback of this fast and cheap method for improvement.

Table 3. Predicted Young's Modulus of Crystals by COMPASS II with Qeq in Forcite Module based on specific faces

force field	charge	number of structures with specific facet Young's modulus	number of unstable Young's modulus	success rate of acquiring results (%)
COMPASS II	Qeq	29	8	72%

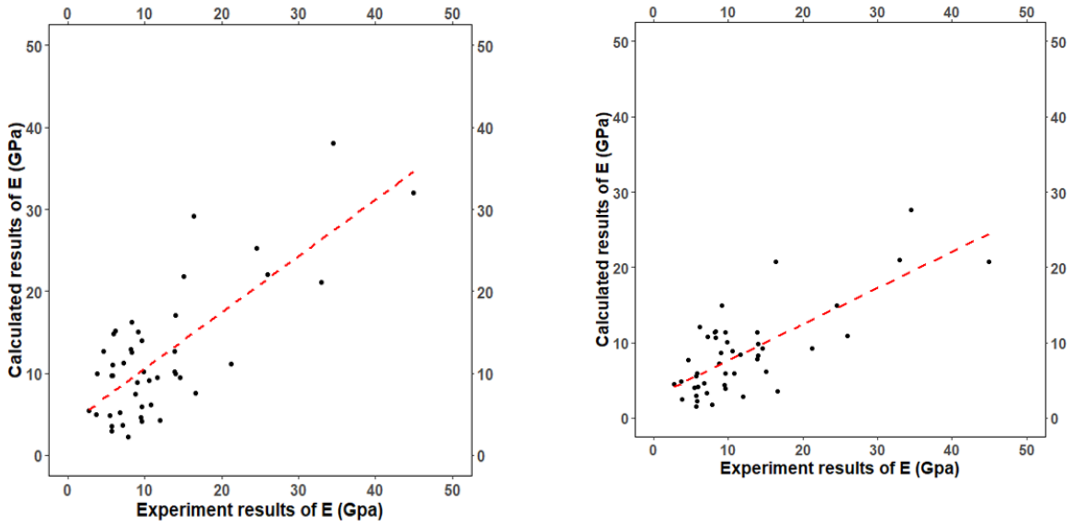

(a) (b)

Figure 17. Young's modulus (*E*) from calculated method versus experiments based on COMPASS II and Qeq: (a) square root mean; (b) harmonic average

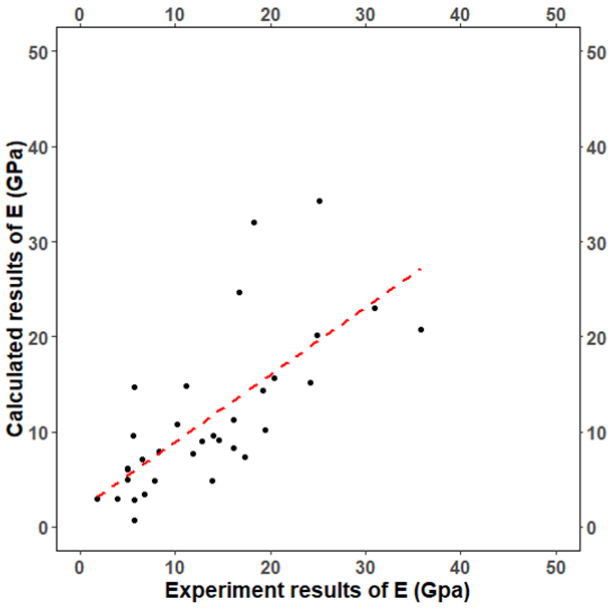

Figure 18. Young's modulus (*E*) from elastic matrices based on COMPASS II Qeq versus experiments

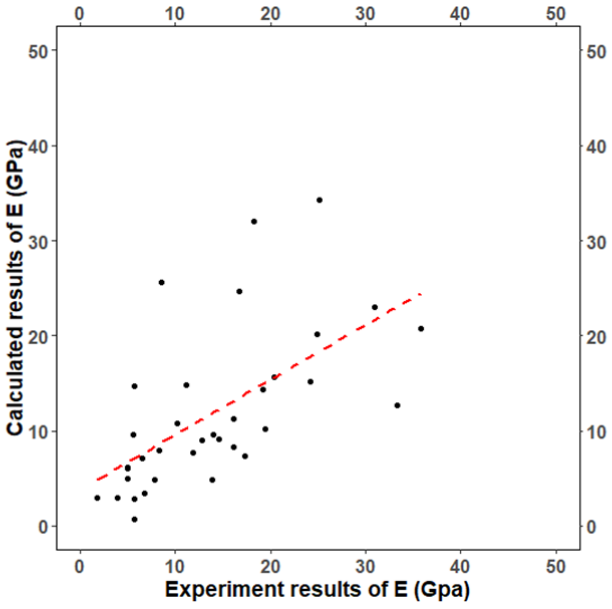

Figure 19. Young's modulus (*E*) from elastic matrices based on COMPASS II Qeq versus experiments without influential points

3.3 Analysis of Young's modulus on specific crystal structures

Single crystals are anisotropic because of the optimal arrangement of atoms within the structure for the efficient use of space[63]. It was expected that the mechanical response would also be distinctive along specific directions resulting from the intramolecular interactions within structures in particular crystallographic directions[43]. In particular, different molecules combined with different crystal packing would lead to the distinctive *E* of this structure, a characteristic of each single crystal. Thus, in contrast to the general analysis, an investigation on specific crystal structure would be more meaningful.

3.3.1 Assessment of Young's modulus on different faces of same crystal

It was common to observe that the same crystal structure had different elastic properties on specific faces. They could manifest significant difference on the value of *E* when an outer strain stress was exerted. The piroxicam form 1 from Mateja *E*gart's work[64] was used as an example to evaluate the accuracy of Forcite modulus simulation on *E* attributes. The combination of forcefield COMPASS II and charge Qeq was used for analysis. Three faces chosen were crystal faces (-1 0 0), (0 1 1) and (0 -1 -1), and their specific facet *E* from elastic matrix.

The comparison of the experiment and prediction is presented in Figure 20. It was found that the experiment values of *E* were all larger than those from the prediction for the same crystal face. This was expected since the slope value of regression line was smaller than 1.

The order of the *E* value on the three chosen crystal faces were same in both methods, indicating a proper description of relative *E* values trend and the crystals' mechanical attributes. However, different from the obvious discrepancy of *E* between face 2 and face 3 from the experiment results, little disparity could be observed from the computational results. The *E* value on face 3 had a significant large gap between the experiment and the simulation. It illustrated that for specific crystal, the Forcite modulus could not provide an overall similar estimation on various faces, indicating a deficiency in assessing the face-based *E* property.

Several reasons for the deficiency include the large variations observed for face 1 and face 3, and small experiment values were displayed in their work, meaning that the experiment results were problematic. Moreover, for this structure, the intermolecular hydrogen bond functioned as a strong intermolecular interaction force and formed a mechanically interlocked structure, playing an important role in the behavior of E[64]. While for the function of forcefield in describing the potential energy, in order to simulate fast, the intramolecular interaction was not thoroughly considered. Interaction such as hydrogen bond were not particularly treated based on crystal structure[59]and structure with interlock characteristics along distinct crystal face orientation was not involved into the description in forcefield, a vital factor affecting the E[64]. Therefore, the predicted *E* values in this crystal structure were smaller than the experiment and the difference on distinct crystal faces was not clearly reflected. Consequently, the Forcite modulus was limited in accurately predicting *E* for specific crystal structures.

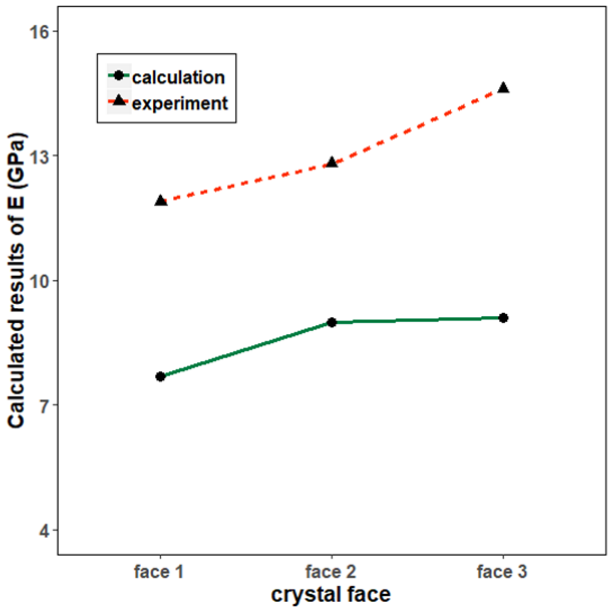

Figure 20. Young's modulus (*E*) of piroxicam form 1 on three different specific faces from experiments and calculation methods

3.3.2 Assessment of Young's modulus on crystal with isotropic response

From the above analysis, the intramolecular interaction within the inner crystal structure could influence the value of *E* and the Forcite module may fail to capture this effect. In order to elucidate the possible shortcoming of this method in predicting *E*, a crystal structure with unique characteristics was selected for assessment. Saccharin, whose *E* values were tested by Reda M. Mohamed[65] was chosen. Although it was a typical monoclinic crystal with different properties along distinct crystal face directions, quite similar *E* values on two major crystal faces – (1 0 0) and (0 1 1) (Table 4) are seen. The possible reasons explained by Varughese[43] could be the combination of van der Waals ($\pi \cdots \pi$) interaction and hydrogen bond on the formation of inner crystal stacks. They explicated that the weak interaction, particularly the hydrogen bonds from the crisscross arrangement of stacked dimers, had an obvious overlap in both face directions, resulting in

the similar stacked structure under strain (Figure 21). Hence, the anisotropy of *E* was reduced along these two crystallographic orientations. This isotropic response from their crystal structure property made it a valuable case to explore the performance of Forcite module in simulating the inner crystal structure characteristics. From the results (Table 4), both *E* from computational methods were smaller than experiments; moreover, the *E* on face (1 0 0) was approximately half of that on face (0 1 1) and little isotropic response could be observed from the two faces.

More detailed analysis was displayed in a 3D *E*-map (Figure 22). It demonstrated that the distribution of *E* was not symmetrical about the middle line of the two faces. It also showed that both *E* were established on the saddle part around the two separate distributed-*E* faces, in accordance with the explanation that these two major faces with relatively weak interaction could easily deformed and release the elastic strain energy[64], but the values of *E*, lack of similarity, were not sufficient to reflect the inner structure similarity of saccharin which was an important structure property for the saccharin crystals. The relatively small prediction value of *E* and the failure of showing the isotropic response of saccharin again indicated the drawback of Forcite module in simulating the intramolecular interactions. Thus, a prefect prediction of Young's modulus on specific structure may not be assessed by Forcite module.

Table 4. Young's modulus results of saccharin on two faces from experiments and computational method

substance	face	Young's modulus from experiments	Young's modulus from computational method
saccharin	(1 0 0)	13.9	4.9
	(0 1 1)	14	9.6

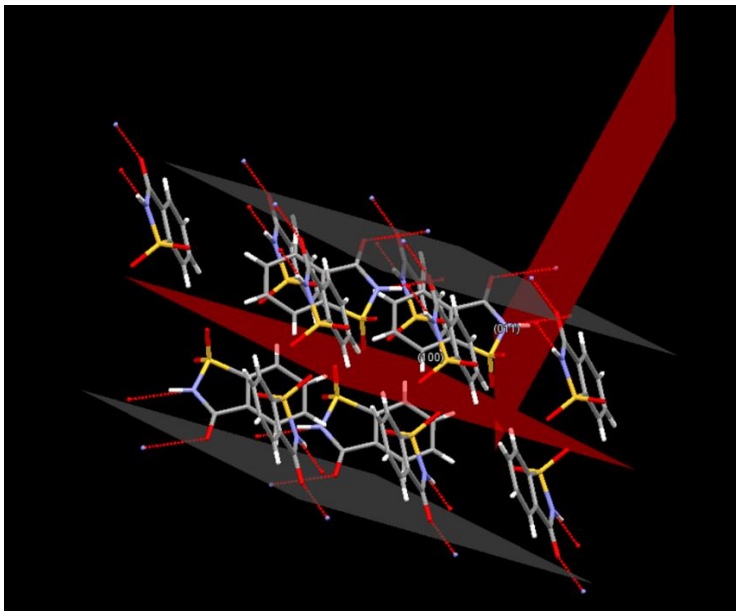

Figure 21. the crystal packing of saccharin and two major faces (1 0 0) and (0 1 1)

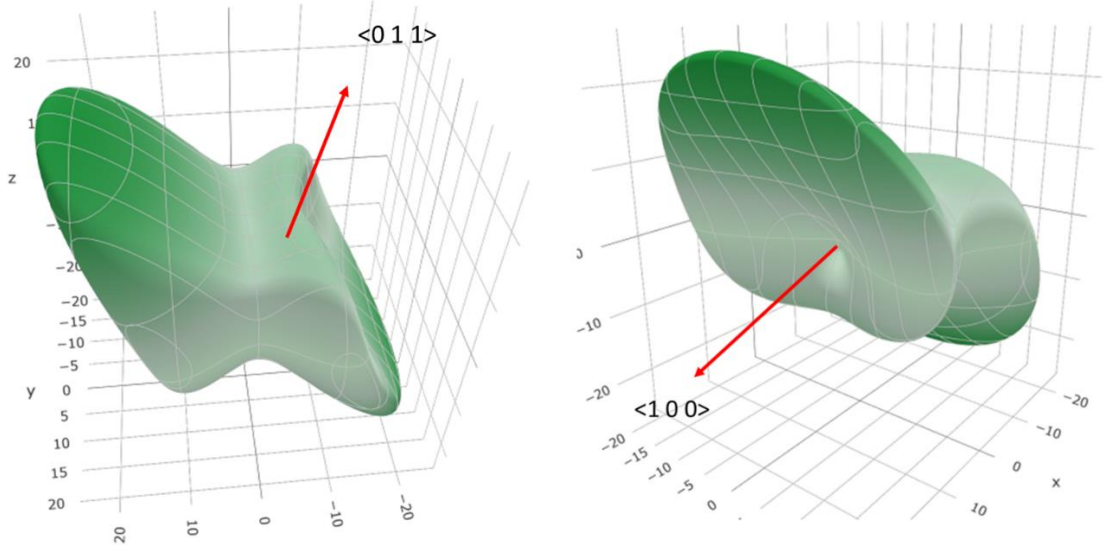

(a) (b)

Figure 22. Three-dimensional distribution of Young's modulus for saccharin on two major faces (a) (0 1 1) and (b) (1 0 0).

3.3.3 Assessment of Young's modulus on polymorphs

It was also helpful to investigate the performance of Forcite module on polymorphs for the influence of intramolecular interaction. The variety in molecular conformation and crystal packing made polymorphs from the same kind molecule a good example to show the influence of intramolecular interactions on the E[66]. Curcumin has three polymorphs and the values of E were examined by Manish Kumar Mishra[67] on specific major face of the crystal structures. As expected, significantly different elastic properties were exhibited on same compound with different crystal structures. The E measured on the major faces of the three structures provided distinct qualification on the elastic property. From their observation, the Form 1 is harder and stiffer compared with the Form 2 and Form 3 and the E was almost twice of the other two forms (Figure 23). When investigating the results of computation, the order of the three forms' E value on major faces was the same as the experiments. However, different from the obvious discrepancy between Form 1 and Form 2 or 3, the prediction result showed a similarity between Form 1 and Form 2, both pronouncedly larger than Form 3. This was conflict with their experiment results and structure analysis on Form 2 and Form 3. From their observation, normal to the major face in both Form 2 and Form 3, few weak intramolecular interactions such as hydrogen bond could be recognized and along the major face, the molecular packing in the two forms were quite similar, leading to the similarity of their elastic response with a relatively small E.

For the results of computation, the defect in simulating the intramolecular interaction, this crystal structure characteristics influence on E was not manifested. Another unanticipated observation from the comparison between experiments and prediction results (Figure 9) was that different from the two above mentioned cases, all the E results from prediction

were larger than those from experiments. Contrast to the performance of Forcite module in reducing intramolecular interaction during simulation, the elastic response seemed to be strengthened in the case of curcumin. This could still be explained by the intramolecular interaction factors. In their work, the Form 2 and Form 3 owned the interlock crystal packing which was expected to increase the intramolecular interaction. However, from a 3-dimenational view, the distance between the two stacked part was large, reducing the interaction force and thus the *E* values were restively small in their experiments. While, for Form 1, due to the existence of macrocylic ring and numerous hydrogen bonds, despite the comparably large distance, the elastic response was still larger compared to the other two forms. As a result, the obvious discrepancy between experiments and simulation illustrated the shortage of Focite modulus function in describing the intramolecular interaction in strength and was insufficient to explore the influence of space arrangement such as interaction distance in a 3D view. Thus, it might not be applicable for a precisely fine prediction.

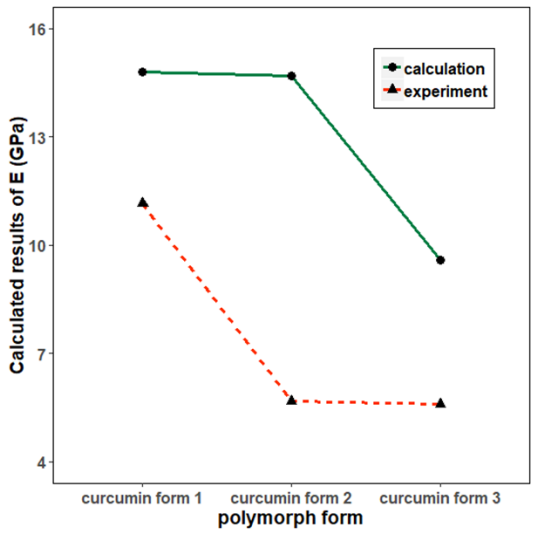

Figure 23. Young's modulus (*E*) of three different curcumin polymorphs on major faces from experiments and calculation methods

4. Discussion

The aim of this study was to evaluate the effect of the Forcite module in Materials Studio 2016 in predicting the Young's modulus from crystal structures. It was expected that if the elastic property could be successfully described from relative strength of both intermolecular and intramolecular interaction within the crystal structures, one may be able to design the formulation by in silicon method and improve the compaction properties with the modification of crystal packing or interaction strength[32, 35-40, 68]. This would be beneficial to the industry manufacturing via the reduction on time and material requirement, especially for new API.

To thoroughly determine the accuracy of the Forcite modulus predictions, we applied all the 10 existing combinations of forcefield and charge to simulation the potential surface energy for the solution of *E*. The success rate of simulation was smaller than 80% and it was speculated that for more pharmaceutical compounds, the successful prediction could not be guaranteed. It was also found that there were several compounds in which the simulation *E* could not be acessed from any of the combinations, such as the LLM-105, β-HMX[69] and famotidine form A[64]. When investigating those crystal characteristics, the common feature was the instability of their structure under strain stress. For the former two compounds, the energetic crystal structures had an easily explosive property, easily being decomposed under suitable conditions[70, 71]. For the famotidine form A, it was not the kinetically favored form of famotidine with relatively denser crystal packing[64]. During the prediction of *E* in Forcite module, an assumed strain stress was exerted on the crystal structure to examine the elastic response. It was reasonably speculated that these crystal

structures could experience fracture in their chemical bonds or crystal packing displacement when the structures were forced to be deformed. Thus, these crystal structures could not sustain the original molecule composition or crystal packing under outer stain stress and fail to estimate the *E* because of the instability. Similarly, very soft structure, such as voriconazole[72], was found failure to predict the *E* and it may result from being unstable under strain stress.

In addition, since the simulation of Forcite module was established on the relative coordinate of each atom within the structure[58], an unambiguous characterization of the crystal structure was a prerequisite for the accurate simulation. Thus, it was anticipated that the structure with characterization problems would be carried forward in simulation of elastic property. One example that could not be assessed was voriconazole fumaric acid cocrystal from Palash Sanphui's work[73]. In their PXRD characterization of this crystal structure, the hydrogen atom of the hydroxyl group could not be located, possibly leading to the failure in the prediction in all the combinations of forcefield and charge. The similar case also found in their work was the voriconazole oxalate salt. Their PXRD pattern was different from the prior reported one[74] and the uncertain structure characterization made it difficult to simulate elastic property.

In spite of these unsolvable structures, our results showed that each combination of forcefield and charge still had a discrepancy on successful predicting *E* from crystal structures and the combination of COMPASS II with Qeq and PCFF with Qeq was first

selected as further exploration method due to the high success rate. This may be because they contained more parameterized atoms and organic compounds against experimental variables[59, 75, 76].

For the two combinations, the different forcefield were developed from the same one – CFF91[59], and thus little disparity could be observed from their comparison with the experiment results based on nanoindentation. Because the COMPASS II was designed based on more parameters of condensed phase properties and the pharmaceutical compounds we researched were mainly in solid state, it was chosen as the optimum combination for further investigation in simulating the elastic property.

When the calculation results from COMPASS II with Qeq were correlated with more compounds via average method, the regression line didn't provide a satisfactory prediction. The adjusted R square was small with an approximate 0.5 value, indicating that the linearity was not strong. Moreover, it was observed that the points scattered randomly in the small *E* value part and some even points deviated largely from the both sides of the regression line. Thus, the Forcite module was unable to provide us with a satisfactory prediction for future application. We analyzed that the poor performance was probably due to the anisotropy of the crystals and simply averaging the *E* values to represent the general elastic property of crystal structures might not be sufficient to be comparable with the experiment results.

To reduce the impact of different faces weights in the expression of *E* by average method, we thus carried out another two statistical methods to explain the results. However, a prediction with decent quality could still not be accessed in both square root mean and harmonic average methods. The relatively small adjusted R square values and slopes in both methods indicated that the limitation of Forcite module in application of simulating the elastic properties. Although the two methods could not provide an ideal prediction, the change of the slope and adjusted R square values in both cases brought to light the fact that the anisotropy of the crystal did influence the elastic behavior of crystals. An independent analysis on specific structure instead of a broad generalization method would be preferred for evaluating the Forcite module.

Considering that the experiment results from nanoindentation was obtained from specific faces of small-volume compounds, we used elastic matrices to estimate the specific facet *E* values. Because each crystal had its own distinct fractional coordinates, the face direction should be transformed into cartesian coordinates for the *E* explanation. The result showed that the slope and adjusted R square were even smaller than the aforementioned methods. The fewer availability of points for comparison could be possible reason, but the distribution of the points suggested that the Forcite module could not provide a convincing prediction via directly simulating the *E* on specific faces when compared with the experiment results. While except for several influential points, the relatively concentrated distribution of most points indeed manifested an improvement of the prediction on *E*. This was probably attributed to the processing of crystal anisotropy. The target crystal direction could be key factor influencing the prediction accuracy.

To clarify the possible influential factors of Forcite module performance, we studied three representative cases. The piroxicam was the case with experiment results on different faces but the same crystal structure. The saccharin had special isotropic response on two different major faces. For the curcumin, it demonstrated disparity of same molecule structure on elastic property with different crystal packing. From the comparisons of three cases, clearly, the simulation on *E* from Forcite modulus was not precise. It was analyzed in each case that underneath the selected crystal direction, the intermolecular and intramolecular interaction within the structure could be one of the determinants on elastic response. For the independent crystal structure, the "interlocked" structure, the distribution of hydrogen bond and the interaction distance on specific crystallographic direction could lead to the different elastic behavior under strain stress. It could be little possible for the Forcite module to simulate such factors simultaneously for distinct crystal system at a very fast speed and many of them were not considered carefully since it was designed for reducing the time consumption and cost[58, 59]. Thus, the accuracy of the prediction could not be guaranteed for the pharmaceutical compounds as the weak interaction played a vital role in affecting the elastic response.

Taken together, the above studies provided us evidence that the current Forcite module might not be a valuable computational tool kit for the prediction of Young's modulus.

5. Conclusion

We have systematically examined the performance of Forcite module from Material Studio 2016 in predicting Young's modulus from crystal structures. From comparison between simulation results and experiment results based on a large number of crystals, we show that this method could be applied to provide prediction on elastic properties. There is a correlation between the prediction and experiments, but the accuracy is limited under different statistical methods. We also established a method to explore the Young's modulus on specific crystal faces from elastic matrix, but still the accuracy is not fine enough to predict the Young's modulus compared with the experiments. It is showed that the limitation on characterizing the inner crystal structures such as the interlocking structure and hydrogen bond interaction strength could be possible reason leading to the coarse prediction results. For achieving more precise simulated results, this method should be optimized and reverified in some parameters such as the intermolecular interaction for further application in pharmaceutical industry.

6. Future work

In the next step, we aim to figure out the crystal systems that can be accurately predicted by the Forcite module method. For these crystal systems, we will try to conclude their crystal characteristics and verify the accuracy with more crystal structures. If the prediction accuracy is acceptable, the Forcite module could be a prospective method for the analysis of mechanical properties in a specific range of crystal systems. Moreover, since the Forcite module developed from the empirical data, validating the model with more experimental is important. Thus, it would be valuable to apply the up-to-date Forcite module trained with more crystal systems for Young's modulus prediction. More parameters associated with the crystal structures could be modified with the selection of the method algorithm for the accuracy increase.

In addition, the computational tool based on density function theory is expected to yield more accurate predictions of *E*. It could be more widely applied once faster computation allows routine access to this technique. This is being evaluated in our lab. Fast and accurate predictions of *E* from crystal structure will be implemented in virtual tablet formulation for new APIs in the future.

7. Bibliography

1. Gibson, M., *Pharmaceutical preformulation and formulation: a practical guide from candidate drug selection to commercial dosage form*. CRC Press: 2016.
2. Herting, M. G.; Kleinebudde, P., Roll compaction/dry granulation: Effect of raw material particle size on granule and tablet properties. *Int J Pharm* **2007,** *338* (1-2), 110-118.
3. Hou, H.; Sun, C. C., Quantifying effects of particulate properties on powder flow properties using a ring shear tester. *J Pharm Sci-Us* **2008,** *97* (9), 4030-4039.
4. Kleinebudde, P., Roll compaction/dry granulation: pharmaceutical applications. *Eur J Pharm Biopharm* **2004,** *58* (2), 317-326.
5. Mangal, S.; Meiser, F.; Morton, D.; Larson, I., Particle Engineering of Excipients for Direct Compression: Understanding the Role of Material Properties. *Curr Pharm Design* **2015,** *21* (40), 5877-5889.
6. Pandey, P.; Bindra, D. S.; Gour, S.; Trinh, J.; Buckley, D.; Badawy, S., Excipient-Process Interactions and their Impact on Tablet Compaction and Film Coating. *J Pharm Sci-Us* **2014,** *103* (11), 3666-3674.
7. Hiestand, E. N., Mechanical properties of compacts and particles that control tableting success. *J Pharm Sci-Us* **1997,** *86* (9), 985-990.
8. Paul, S.; Sun, C. C., Modulating Sticking Propensity of Pharmaceuticals Through Excipient Selection in a Direct Compression Tablet Formulation. *Pharm Res-Dordr* **2018,** *35* (6).
9. Akseli, I.; Stecula, A.; He, X. R.; Ladyzhynsky, N., Quantitative Correlation of the Effect of Process Conditions on the Capping Tendencies of Tablet Formulations. *J Pharm Sci-Us* **2014,** *103* (6), 1652-1663.
10. Hiestand, E. N., Principles, tenets and notions of tablet bonding and measurements of strength. *Eur J Pharm Biopharm* **1997,** *44* (3), 229-242.
11. Fell, J. T.; Newton, J. M., Determination of Tablet Strength by Diametral-Compression Test. *J Pharm Sci-Us* **1970,** *59* (5), 688-&.
12. Fahr, A., *Voigt's Pharmaceutical Technology*. John Wiley & Sons: 2017.
13. Shafer, E. G. E.; Wollish, E. G.; Engel, C. E., The Roche Friabilator. *J Am Pharm Assoc* **1956,** *45* (2), 114-116.
14. Sinka, I. C.; Cunningham, J. C.; Zavaliangos, A., Analysis of tablet compaction. II. Finite element analysis of density distributions in convex tablets. *J Pharm Sci-Us* **2004,** *93* (8), 2040-2053.
15. Porter, S.; Sackett, G.; Liu, L., Chapter 33 - Development, Optimization, and Scale-up of Process Parameters: Pan Coating. In *Developing Solid Oral Dosage Forms*, Qiu, Y.; Chen, Y.; Zhang, G. G. Z.; Liu, L.; Porter, W. R., Eds. Academic Press: San Diego, 2009; pp 761-805.
16. Hiestand, H. E. N.; Smith, D. P., Indexes of Tableting Performance. *Powder Technol* **1984,** *38* (2), 145-159.
17. Sun, C. C., Decoding Powder Tabletability: Roles of Particle Adhesion and Plasticity. *J Adhes Sci Technol* **2011,** *25* (4-5), 483-499.
18. Osei-Yeboah, F.; Chang, S. Y.; Sun, C. C., A critical Examination of the Phenomenon of Bonding Area - Bonding Strength Interplay in Powder Tableting. *Pharm Res-Dordr* **2016,** *33* (5), 1126-1132.
19. Galen, S.; Zavaliangos, A., Strength anisotropy in cold compacted ductile and brittle powders. *Acta Mater* **2005,** *53* (18), 4801-4815.
20. Sun, C. C., Materials Science Tetrahedron-A Useful Tool for Pharmaceutical Research and Development. *J Pharm Sci-Us* **2009,** *98* (5), 1671-1687.

21. Santos, H. M. M.; Sousa, J. J. M. S., Tablet Compression. *Pharmaceutical Sciences Encyclopedia* **2010**, 1-32.
22. Chapter 2 - Agglomerate Bonding. In *Handbook of Powder Technology*, Capes, C. E., Ed. Elsevier Science B.V.: 1980; Vol. 1, pp 23-51.
23. Gad, S. C., *Pharmaceutical Manufacturing Handbook: Production and Processes*. John Wiley & Sons: 2007.
24. Mazel, V.; Diarra, H.; Malvestio, J.; Tchoreloff, P., Lamination of biconvex tablets: Numerical and experimental study. *Int J Pharm* **2018,** *542* (1-2), 66-71.
25. Tye, C. K.; Sun, C. C.; Amidon, G. E., Evaluation of the effects of tableting speed on the relationships between compaction pressure, tablet tensile strength, and tablet solid fraction. *J Pharm Sci-Us* **2005,** *94* (3), 465-472.
26. Long, W. M., RADIAL PRESSURES IN POWDER COMPACTION. *Powder Metallurgy* **1960,** *3* (6), 73-86.
27. Davies, P., *Oral Solid Dosage Forms, in Pharmaceutical Preformulation and Formulation*. Informa Healthcare, Inc: 2009; p 367–430.
28. Roberts, R. J., *Particulate Analysis: Mechanical properties, in Solid State Characterization of Pharmaceuticals*. John Wiley & Sons: 2011; p 357–

369.
29. Nordstrom, J.; Kievan, I.; Alderborn, G., A protocol for the classification of powder compression characteristics. *Eur J Pharm Biopharm* **2012,** *80* (1), 209-216.
30. B. B. Sheth, F. J. B., and R. F. Shangraw, *Tablets, in Pharmaceutical Dosage Forms*. Marcel Dekker: 1980; p 109–185.
31. Jain, S., Mechanical properties of powders for compaction and tableting: an overview. *Pharmaceutical Science & Technology Today* **1999,** *2* (1), 20-31.
32. Sun, C. Q.; Grant, D. J. W., Influence of crystal structure on the tableting properties of sulfamerazine polymorphs. *Pharm Res-Dordr* **2001,** *18* (3), 274-280.
33. Roberts, R. J.; Rowe, R. C.; York, P., The relationship between Young's modulus of elasticity of organic solids and their molecular structure. *Powder Technol* **1991,** *65* (1), 139-146.
34. Roberts, R. J.; Rowe, R. C.; York, P., The Relationship between Indentation Hardness of Organic-Solids and Their Molecular-Structure. *J Mater Sci* **1994,** *29* (9), 2289-2296.
35. Feng, Y. S.; Grant, D. J. W.; Sun, C. C., Influence of crystal structure on the tableting properties of n-alkyl 4-hydroxybenzoate esters (Parabens). *J Pharm Sci-Us* **2007,** *96* (12), 3324-3333.
36. Sun, C. Q.; Grant, D. J. W., Improved tableting properties of p-hydroxybenzoic acid by water of crystallization: A molecular insight. *Pharm Res-Dordr* **2004,** *21* (2), 382-386.
37. Sun, C. C.; Hou, H., Improving mechanical properties of caffeine and methyl gallate crystals by cocrystallization. *Cryst Growth Des* **2008,** *8* (5), 1575-1579.
38. Chattoraj, S.; Shi, L. M.; Sun, C. C., Understanding the relationship between crystal structure, plasticity and compaction behaviour of theophylline, methyl gallate, and their 1: 1 co-crystal. *Crystengcomm* **2010,** *12* (8), 2466-2472.
39. Khomane, K. S.; More, P. K.; Raghavendra, G.; Bansal, A. K., Molecular Understanding of the Compaction Behavior of Indomethacin Polymorphs. *Mol Pharmaceut* **2013,** *10* (2), 631-639.
40. Chattoraj, S.; Shi, L. M.; Chen, M.; Alhalaweh, A.; Velaga, S.; Sun, C. C., Origin of Deteriorated Crystal Plasticity and Compaction Properties of a 1:1 Cocrystal between Piroxicam and Saccharin. *Cryst Growth Des* **2014,** *14* (8), 3864-3874.
41. Higuchi, T.; Elowe, L. N.; Busse, L. W., The Physics of Tablet Compression .5. Studies on Aspirin, Lactose, Lactose-Aspirin, and Sulfadiazine Tablets. *J Am Pharm Assoc Sci* **1954,** *43* (11), 685-689.
42. Saha, S.; Desiraju, G. R., Crystal Engineering of Hand-Twisted Helical Crystals. *Journal of the American Chemical Society* **2017,** *139* (5), 1975-1983.

43. Varughese, S.; Kiran, M. S. R. N.; Ramamurty, U.; Desiraju, G. R., Nanoindentation in Crystal Engineering: Quantifying Mechanical Properties of Molecular Crystals. *Angew Chem Int Edit* **2013,** *52* (10), 2701-2712.
44. Roberts, R. J.; Payne, R. S.; Rowe, R. C., Mechanical property predictions for polymorphs of sulphathiazole and carbamazepine. *Eur J Pharm Sci* **2000,** *9* (3), 277-283.
45. Payne, R. S.; Roberts, R. J.; Rowe, R. C.; McPartlin, M.; Bashal, A., The mechanical properties of two forms of primidone predicted from their crystal structures. *Int J Pharm* **1996,** *145* (1-2), 165-173.
46. Sun, W. J.; Kothari, S.; Sun, C. C., The relationship among tensile strength, Young's modulus, and indentation hardness of pharmaceutical compacts. *Powder Technol* **2018,** *331*, 1-6.
47. Sun, C. Q.; Grant, D. J. W., Influence of elastic deformation of particles on Heckel analysis. *Pharm Dev Technol* **2001,** *6* (2), 193-200.
48. Modules tutorials, Materials Studio 2017. 2017.
49. Raut, D.; Kiran, M. S. R. N.; Mishra, M. K.; Asiri, A. M.; Ramamurty, U., On the loading rate sensitivity of plastic deformation in molecular crystals. *Crystengcomm* **2016,** *18* (20), 3551-3555.
50. Kiran, M. S. R. N.; Varughese, S.; Reddy, C. M.; Ramamurty, U.; Desiraju, G. R., Mechanical Anisotropy in Crystalline Saccharin: Nanoindentation Studies. *Cryst Growth Des* **2010,** *10* (10), 4650-4655.
51. Varughese, S.; Kiran, M. S. R. N.; Solanko, K. A.; Bond, A. D.; Ramamurty, U.; Desiraju, G. R., Interaction anisotropy and shear instability of aspirin polymorphs established by nanoindentation. *Chem Sci* **2011,** *2* (11), 2236-2242.
52. Liao, X. M.; Wiedmann, T. S., Measurement of process-dependent material properties of pharmaceutical solids by nanoindentation. *J Pharm Sci-Us* **2005,** *94* (1), 79-92.
53. Egart, M.; Jankovic, B.; Srcic, S., Application of instrumented nanoindentation in preformulation studies of pharmaceutical active ingredients and excipients. *Acta Pharmaceut* **2016,** *66* (3), 303-330.
54. Oliver, W. C.; Pharr, G. M., An Improved Technique for Determining Hardness and Elastic-Modulus Using Load and Displacement Sensing Indentation Experiments. *J Mater Res* **1992,** *7* (6), 1564-1583.
55. http://web.mit.edu/16.20/homepage/3_Constitutive/Constitutive_files/module_3_with_solutions.pdf.
56. Gaillac, R.; Pullumbi, P.; Coudert, F. X., ELATE: an open-source online application for analysis and visualization of elastic tensors. *J Phys-Condens Mat* **2016,** *28* (27).
57. Ashcroft, N. W.; Mermin, N. D., *Solid state physics*. Saunders College: 1976.
58. Maple, J. R.; Dinur, U.; Hagler, A. T., Derivation of force fields for molecular mechanics and dynamics from ab initio energy surfaces. *Proc Natl Acad Sci U S A* **1988,** *85* (15), 5350-5354.
59. Sun, H., COMPASS: An ab Initio Force-Field Optimized for Condensed-Phase ApplicationsOverview with Details on Alkane and Benzene Compounds. *The Journal of Physical Chemistry B* **1998,** *102* (38), 7338-7364.
60. Dunitz, J. D.; Gavezzotti, A., Attractions and repulsions in molecular crystals: What can be learned from the crystal structures of condensed ring aromatic hydrocarbons? *Accounts Chem Res* **1999,** *32* (8), 677-684.
61. Paulini, R.; Muller, K.; Diederich, F., Orthogonal multipolar interactions in structural chemistry and biology. *Angew Chem Int Edit* **2005,** *44* (12), 1788-1805.
62. Metrangolo, P.; Neukirch, H.; Pilati, T.; Resnati, G., Halogen bonding based recognition processes: A world parallel to hydrogen bonding. *Accounts Chem Res* **2005,** *38* (5), 386-395.
63. Kitaigorodsky, A. I., *Molecular Crystals and Molecules* Academic Press: 1973.

64. Egart, M.; Jankovic, B.; Lah, N.; Ilic, I.; Srcic, S., Nanomechanical Properties of Selected Single Pharmaceutical Crystals as a Predictor of Their Bulk Behaviour. *Pharm Res-Dordr* **2015,** *32* (2), 469-481.
65. Mohamed, R. M.; Mishra, M. K.; Al-Harbi, L. M.; Al-Ghamdi, M. S.; Ramamurty, U., Anisotropy in the mechanical properties of organic crystals: temperature dependence. *Rsc Adv* **2015,** *5* (79), 64156-64162.
66. Ribeiro, A. P. B.; Masuchi, M. H.; Miyasaki, E. K.; Domingues, M. A. F.; Stroppa, V. L. Z.; de Oliveira, G. M.; Kieckbusch, T. G., Crystallization modifiers in lipid systems. *J Food Sci Technol* **2015,** *52* (7), 3925-3946.
67. Mishra, M. K.; Sanphui, P.; Ramamurty, U.; Desiraju, G. R., Solubility-Hardness Correlation in Molecular Crystals: Curcumin and Sulfathiazole Polymorphs. *Cryst Growth Des* **2014,** *14* (6), 3054-3061.
68. Khomane, K. S.; More, P. K.; Bansal, A. K., Counterintuitive Compaction Behavior of Clopidogrel Bisulfate Polymorphs. *J Pharm Sci-Us* **2012,** *101* (7), 2408-2416.
69. Kucheyev, S. O.; Gash, A. E.; Lorenz, T., Deformation and fracture of LLM-105 molecular crystals studied by nanoindentation. *Mater Res Express* **2014,** *1* (2).
70. Armstrong, R. W.; Elban, W. L., Materials science and technology aspects of energetic (explosive) materials. *Mater Sci Tech-Lond* **2006,** *22* (4), 381-395.
71. Pagoria, P. F.; Lee, G. S.; Mitchell, A. R.; Schmidt, R. D., A review of energetic materials synthesis. *Thermochim Acta* **2002,** *384* (1-2), 187-204.
72. Butters, M.; Ebbs, J.; Green, S. P.; MacRae, J.; Morland, M. C.; Murtiashaw, C. W.; Pettman, A. J., Process development of voriconazole: A novel broad-spectrum triazole antifungal agent. *Org Process Res Dev* **2001,** *5* (1), 28-36.
73. Sanphui, P.; Mishra, M. K.; Ramamurty, U.; Desiraju, G. R., Tuning Mechanical Properties of Pharmaceutical Crystals with Multicomponent Crystals: Voriconazole as a Case Study. *Mol Pharmaceut* **2015,** *12* (3), 889-897.
74. Bodapati, V. R. A. J. G. A. K. S. R. M. A. S. R. Process for preparation of novel salt of voriconazole oxalate form. 2007.
75. Bunte, S. W.; Sun, H., Molecular Modeling of Energetic Materials: The Parameterization and Validation of Nitrate Esters in the COMPASS Force Field. *The Journal of Physical Chemistry B* **2000,** *104* (11), 2477-2489.
76. McQuaid, M. J.; Sun, H.; Rigby, D., Development and validation of COMPASS force field parameters for molecules with aliphatic azide chains. *J Comput Chem* **2004,** *25* (1), 61-71.